Hydrogen vacancies facilitate hydrogen transport kinetics in sodium hydride nanocrystallites

S. Singh* and S. W. H. Eijt

Department of Radiation, Radionuclides, and Reactors, Fundamental Aspects of Materials and Energy, Faculty of Applied Sciences, Delft University of Technology, Mekelweg 15, 2629 JB Delft, The Netherlands

(Received 17 October 2008; revised manuscript received 28 November 2008; published 30 December 2008)

We report *ab initio* calculations based on density-functional theory, of the vacancy-mediated hydrogen migration energy in bulk NaH and near the NaH(001) surface. The estimated rate of the vacancy-mediated hydrogen transport, obtained within a hopping diffusion model, is consistent with the reaction rates of H-D exchange in nano-NaH at the relatively low temperatures observed in recent neutron studies on $TiCl_3$-doped $NaAlH_4$. We further obtained the formation energy for hydrogen vacancies and interstitials in NaH in all relevant charged states. These formation energies are too high to lead to the abundant hydrogen concentrations seen experimentally. *Ab initio* calculations on the NaCl//NaH interface are presented to provide an insight into the mechanism which may lead to high hydrogen concentrations. We show that the formation of an fcc-Na interlayer during the growth of NaH on top of NaCl is plausible, providing a source of vacancies and leading to fast hydrogen transport. The low interface energies for NaCl//NaH are consistent with an easy growth of NaH crystallites on NaCl nucleation centers, which may, therefore, act as grain refiners.

DOI: 10.1103/PhysRevB.78.224110 PACS number(s): 61.72.jd, 63.20.dk, 66.30.Pa

I. INTRODUCTION

Hydrogen is a promising candidate to solve future sustainable energy supply problems because of its environmental friendliness, abundant availability, and high energy content.[1] However, no material meets the international targets yet. A good hydrogen storage system should have a satisfactorily fast hydrogen release and uptake kinetics, and simultaneously meet other stringent storage conditions such as high gravimetric and volumetric densities, and reversibility of the hydrogen desorption reactions.

Sodium alanate ($NaAlH_4$) is a potential hydrogen storage system with a theoretical 5.6 wt % hydrogen capacity, releasing hydrogen in two steps. Addition of Ti compounds [such as $TiCl_3$, $Ti(OBu)_4$, or Ti nanoparticles] makes these reactions reversible with a large decrease in decomposition temperatures, and increases the reaction kinetics significantly,[2,3] at the cost of a slight decrease in the hydrogen capacity. The addition of such catalysts leads to a hydrogen uptake and release of ~4.5 wt % in practice. A number of recent experiments and calculations indicated that Ti facilitates the reaction kinetics and reversibility by inducing the presence of hydrogen vacancies in $NaAlH_4$.[4,5] We recently discovered that $TiCl_3$ has a further important role as a grain refiner[6] besides acting as a hydrogen splitter.[2,3,7] Moreover, a pronounced hydrogen-vacancy formation in the decomposition products such as Na_3AlH_{6-x} (approximately 20%) and NaH_{1-x} ($\geq$3%) was detected in the neutron-scattering study on $TiCl_3$-doped and nanostructured $NaAlH_4$.[6] Recent studies on hydrogen and lithium insertion materials, i.e., nano-MgH_{2-x} and nano-Li_xTiO_2, respectively, revealed that samples with nanosized crystallites may contain very high hydrogen-vacancy concentrations and a largely increased lithium solubility.[8–10]

Further, an unexpected, clear, and relatively fast H-D exchange was observed in the nano-NaH_{1-x} phase in the neutron study.[6] H-D exchange in nanostructured NaH was recently also observed in dynamic exchange experiments using low external hydrogen pressures of the order of a few millibars.[11] In contrast, this exchange was absent in vacancy deprived large crystallites of undoped $NaAlH_4$.[6] It is known that Ti is not incorporated in the NaH nanoparticles[12] and mechanisms explaining the relatively fast hydrogen transport in the NaH nanoparticles involving Ti can, therefore, be largely excluded. We believe that the transport kinetics and H-D exchange is directly related to the presence of abundant vacancy defects in the nano-NaH phase. The presence of crystal defects is known to have a significant effect on the diffusion of atoms and ions.[13–15] They will, therefore, affect the mass transport in the materials in a direct manner, which is of large significance for the reversibility of the hydrogenation reactions. This paper presents *ab initio* calculations which support this mechanism. In particular, we studied in details the relevant migration energies as they control the diffusion and magnitude of the diffusion coefficient for atomic hydrogen in the presence of hydrogen vacancies (V_H) in the NaH lattice. We, further, obtained the formation energies for various hydrogen defects (vacancies V_H and interstitials H_i) in the NaH lattice in all possible charged states $(+1,0,-1)$.[16] Various charge states of the defects need to be considered, as the defects introduce additional energy levels in the band structure of this ionic salt host material consisting of Na^+ and H^- ions. Finally, we evaluated a model on the interface of NaH with NaCl, the latter acting as a nucleation center, to explain the significant amount of hydrogen vacancies in nano-NaH observed experimentally upon hydrogen cycling of the $TiCl_3$-doped $NaAlH_4$ hydrogen storage system. The model shows that the formation of an in-between fcc-Na layer is preferred, providing a source for the detected high vacancy concentrations.

II. COMPUTATIONAL PROCEDURE

Ab initio calculations, based on density-functional theory (DFT),[17,18] were carried out using ultrasoft pseudopotentials (USPPs) (Ref. 19) and the generalized gradient approxima-

tion (GGA).[20,21] The calculations were implemented in the Vienna *Ab initio* Simulation Package (VASP) code.[22] Ultrasoft potentials with the valence states 3*s* for Na, 1*s* for H, and 3*s* and 3*p* for Cl were used. The geometry optimization calculations were performed with a 200 and 219.242 eV energy cutoff for NaH and sodium chloride (NaCl), respectively, with the convergence criterion set at 2×10^{-5} eV atom^{-1}. The Brillouin zone was sampled using a Monkhorst-Pack sampling technique.[23] A $5\times5\times5$ grid was used for bulk NaH, Na, and NaCl using a 64 atom supercell, while $6\times6\times1$ and $9\times9\times1$ *k*-point grids were used for the NaH surface (001) (160 atoms) and NaCl//NaH (001) (320 atoms and 40 atoms) interface calculations, respectively. The equilibrium atomic positions after relaxation of the structure were calculated starting from bulk positions using the refined crystallographic data from Refs. 24 and 25 and the unit-cell parameters were validated by optimizing the unit cell. The calculated unit-cell parameters showed minor and expected deviations relative to the experimental values for bulk single crystals of 3% for NaH (experimental 4.89 Å, calculated 4.73 Å), 4% for face-centered-cubic (fcc) Na (expected 5.33 Å, calculated 5.10 Å), and 3% for NaCl (experimental 5.63 Å, calculated 5.47 Å). The band gap E_g of 3.51 eV for bulk NaH deduced from our calculations is 3% smaller than obtained in a recent other DFT-based study,[26] employing projector augmented wave (PAW) potentials. This small difference may be the result of the larger lattice parameter of 4.82 Å and the PAW potentials for the interaction between ions and electrons used in the latter study. We obtained a very similar overall electron energy density of states (DOS).

After calculating the equilibrium structure and total energy of the perfect crystal, a hydrogen vacancy (V_H) was introduced into an otherwise perfect lattice. We calculated the formation energies for hydrogen-related defects in all charged states $(+1,0,-1)$ for bulk NaH. We compared this energy with the energy to create a vacancy at the NaH(001) surface to examine the influence of nanoscale dimensions on the formation energy for a vacancy. Further, migration energies were calculated to study the diffusion through bulk NaH and the near-surface layers of NaH. Additionally, we also studied the migration energy for an isolated hydrogen atom in fcc-Na. All bulk and interface calculations were performed with and without relaxation of selected Na atoms around the defect, while the surface calculations were done without relaxation of atoms.

The energy costs to introduce a defect, i.e., the formation energy of the respective defect E^f, into a perfect lattice was calculated using the following expression:[27,28]

$$E^f = E_{\text{tot}}(D^q) - E_{\text{tot}}(\text{bulk}) \pm \mu_H + qE_F, \tag{1}$$

where the first and second term are the total energies of supercells with and without a defect, respectively. μ_H is the chemical potential of hydrogen at $T=0$, which is fixed to half of the energy of an H_2 molecule, i.e., 2.21 eV. The sign of the μ_H term is positive if a hydrogen vacancy is created and negative in case a hydrogen interstitial is created. The last term in Eq. (1) relates to charged defects, q is the charge of the defect, and E_F is the energy of the reservoir with which these charges are exchanged, i.e., the Fermi energy level or the electron chemical potential. The equilibrium concentration c of a defect at a given temperature T, with k_B the Boltzmann constant, can be calculated using the expression

$$c = \exp\left(\frac{-E^f}{k_B T}\right). \tag{2}$$

Further, we calculated the energy and relaxed geometry for a set of different interfaces, including the Na//NaH (30 atoms), NaCl//Na (30 atoms), and NaCl//NaH (40 atoms) (001) interfaces, motivated by the growth of NaH on NaCl crystallites acting as nucleation centers, as described by Singh *et al.*[6] The interface energy is defined as the difference in the energy of an interface system relative to the energies of the involved bulk crystals, as given below:

$$E_{\text{int}} = E(\text{interface system}) - \sum E(\text{bulk crystals}). \tag{3}$$

III. RESULTS AND DISCUSSION

A. Migration energies and diffusion coefficients of hydrogen vacancies

The hydrogenation kinetics of a hydrogen storage material is often rate limited by a diffusion-controlled reaction and transport, determining the effective velocity at which the hydrogen atoms can diffuse through the solid matrix. We applied a hopping model to mimic the vacancy-mediated hydrogen diffusion in fcc-NaH.

Based on the hopping diffusion model, a hydrogen atom (neighboring a vacancy) is thermally excited and vibrates around its equilibrium position. This vibrational motion has a frequency ν_0, which is material dependent, and is typically of the order of $10^{12}-10^{13}$ s^{-1}. For each of the vibrational cycles, a finite and small probability of hopping into the neighboring vacant lattice site exists, which depends on the relative magnitude of the energy barrier height E_m (the migration energy) and the thermal vibrational energy k_BT. The diffusing atom needs to cross this E_m in order to reach the vacancy by pushing the surrounding atoms apart and squeezing through. This process is facilitated when more than one neighboring lattice sites are vacant. However, our calculations consider the tractable case of hopping into an isolated hydrogen vacancy, which is strictly valid in the limit of low vacancy concentrations.

Mathematically, the model is represented by the expressions given in Eqs. (4) and (5) below for the diffusion constant, where the factor 1/6 takes care of the three-dimensional (3D) bidirectional motion in the fcc sublattice and S is the distance which a diffusing atom covers to reach the vacancy (see Fig. 1 for the case of NaH). The concentration of vacancies c, in thermal equilibrium, is given by Eq. (2). The diffusion constant defined in Eqs. (4) and (5) can be used to calculate the characteristic diffusion time t, given in Eq. (6), for hydrogen to move out of or into a grain of radius R,

$$D = \frac{1}{6}S^2\nu_0 c\,\exp(-E_m/k_BT), \tag{4}$$

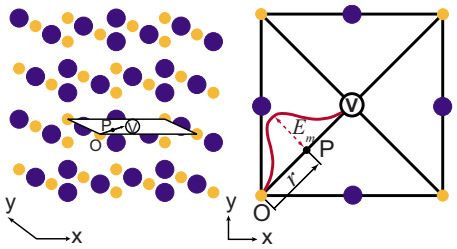

FIG. 1. (Color online) A schematic diagram showing the hydrogen path to a neighboring hydrogen vacancy used in the calculations. The selected ten Na atoms neighboring the vacancy were allowed to relax. Small circles (filled with orange color) represent hydrogen atoms and large filled circles (in dark blue) represent Na atoms. The open circle containing *V* represents an isolated hydrogen vacancy.

$$D_0 = \frac{1}{6} S^2 \nu_0, \tag{5}$$

$$t = R^2/6D. \tag{6}$$

These equations are strictly valid for the diffusion of an isolated vacancy solely, since the related diffusion motion of the hydrogen atoms is correlated because the chance of hopping back into the original lattice position is larger than toward other positions. This can be accounted for by a correlation factor f which is of order ≤ 1, which has been discarded here. For the comparison with experiments, we are primarily interested in obtaining the correct order of magnitude of the diffusion time scale rather than a model dependent exact value.

For NaH, we calculated the migration energy for the hydrogen vacancy in all possible charged states with and without selective atomic relaxation. This is achieved by calculating the cohesive energy of the 63 atom supercell for different positions of hydrogen on the path toward the hydrogen vacancy moving along the ⟨110⟩ NaH diagonal (see Fig. 1). The neighboring ten Na atoms around the vacancy were allowed to relax. The hydrogen migration energy E_m in the presence of a vacancy was deduced from the resulting curve, shown in Fig. 2 for a neutral vacancy. E_m is the difference in energy at point *O* and at the saddle point *P* and is 0.94 eV for the case of a neutral vacancy. This is significantly lower than for the case of a direct exchange of hydrogen with one of its neighboring hydrogen atoms, i.e., in absence of a vacancy, with a calculated migration energy of 4.05 eV. Further, we estimated the attempt frequency from the same curve by a parabolic fit near the equilibrium position *O* using Eq. (7) with k the force constant of the locally harmonic hydrogen vibration,

$$E = \frac{1}{2} k r^2, \tag{7}$$

$$\nu_0 = 1/2\pi\sqrt{k/m}. \tag{8}$$

We verified that the lattice point *O* indeed corresponds to a local minimum, and point *P* is a saddle point, by calculating the total energy as a function of displacement of the hydrogen atom in directions perpendicular to the line connecting the lattice point *O* and saddle point *P*. We note that the obtained frequencies of 17–18 THz (Table I) are situated in the lower part of the high-frequency interval of hydrogen dominated vibrations in the phonon densities of states (p-DOS) for bulk NaH calculated by Ke and Tanaka.[26]

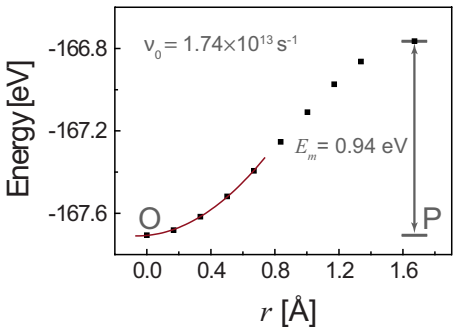

FIG. 2. (Color online) Calculated total energy as a function of H position along the direct path of hydrogen toward the neighboring hydrogen vacancy in bulk NaH. The local minimum at point *O* was fitted by a parabola for the estimation of the local hydrogen vibration frequency. The red line represents the fit.

The hopping model was used to assess the diffusion coefficients for the various types of vacancies. Subsequently, the characteristic diffusion time was deduced for hydrogen to cover a given distance, corresponding to an average NaH grain size of 60 nm in radius (see Table I). For the neutral vacancy, we, thus, found that the time needed for hydrogen to cover this distance at 420 K at the experimentally observed vacancy concentration of 3% (minimum) is 950 s, i.e., in agreement, to at least within the correct order of magnitude, with the time scale of H-D exchange observed in neutron-diffraction measurements.[6] Clearly, the migration energy of 4 eV, in absence of vacancies, leads to negligible hydrogen diffusion at this temperature and time scales, showing that vacancies are crucial for H-D exchange in NaH at 420 K. As expected for isolated hydrogen atoms in fcc-Na, the hydrogen diffusion is here much faster with a diffusion time of the order of approximately 6.7×10^{-4} s only, showing the high mobility of hydrogen in fcc-Na. Our calculations further show that the positively charged vacancy V_H^+ has the lowest migration energy among the three possible types of isolated vacancies in NaH. Therefore, once they are formed, V_H^+ will induce the fastest hydrogen diffusion rate. In

TABLE I. Migration energy for hydrogen in the presence of the various charged vacancies (+1,0,−1) in NaH including local structure relaxation and the corresponding characteristic diffusion time for hydrogen to cover a diffusion distance of 60 nm at a temperature of 420 K.

	V_H^0	V_H^+	V_H^-
ν_0 (10^{13} s^{-1})	1.74	1.72	1.77
E_m (eV)	0.94	0.57	1.17
D (nm^2 s^{-1})	0.63	1.7×10^4	1.29×10^{-3}
t (s)	~950	~0.21	$\sim4.5\times10^5$

TABLE II. Formation energies of the H vacancy in the various charged states in bulk NaH and at the NaH(001) surface, calculated with the Fermi energy at 0 eV, i.e., equal to the top of the valence band.

	Formation energy (eV)		
Type of vacancy	$Bulk_{unrelaxed}$	$Bulk_{relaxed}$	$Surface_{unrelaxed}$
V_H^0	2.66	2.61	2.47
V_H^+	1.18	0.68	3.21
V_H^-	4.98	4.93	3.59

order to cover the distance of a grain radius at 420 K, a V_H^+ vacancy concentration of only 5.6×10^{-6} would be needed in order to attain a diffusion time of the order of 950 s. Based on the formation energy of 0.68 eV, as presented in more detail in Sec. III B, an equilibrium concentration of 7.1×10^{-9} at 420 K is derived, i.e., still lower by 2–3 orders of magnitude. Nevertheless, this shows that, once they are formed, these positively charged vacancies will be highly mobile and can easily travel macroscopic distances at suitable hydrogen cycling temperatures and increase the reaction kinetics in light-metal hydrides significantly. We note that the diffusion time would be somewhat larger for the case of deuterium atoms—used, for example, in monitoring the H-D exchange processes—by of the order of $\sqrt{2}$ as of their higher mass.

Considering the effect of the local hydrogen migration energy, we finally remark that our calculations on the unrelaxed NaH(001) surface indicate that hydrogen moves more easily inward, deeper into the NaH subsurface region, than outwards to the top NaH layer. The obtained migration energy for a hydrogen atom to move from the second layer to the top NaH layer is, namely, 1.37 eV in the presence of a neutral vacancy, while E_m for the reverse motion from the top layer inward to the below layer is only 1.22 eV, induced by the weaker binding of the hydrogen atom in the topmost layer.

B. Comparison of formation energy of different types of defects

Clearly, the formation energy of hydrogen vacancies is an important factor in determining the vacancy concentrations present in the material. This formation energy, together with a vacancy specific hydrogen migration energy, will be the dominant factor in determining the activation energy for diffusion, and correspondingly, the hydrogen kinetics. Therefore, in the next sections we focus on the formation energies of hydrogen vacancies and interstitials in the various charge states. Further, we evaluate a model relevant for explaining large vacancy concentrations in metal hydride nanoparticles in general and find that this mechanism can induce the high hydrogen-vacancy concentrations in the specific case of NaH nanoparticles resulting during the hydrogen desorption reactions of $TiCl_3$-doped $NaAlH_4$.

Table II presents the formation energies of neutral and charged vacancies in bulk NaH before and after structural relaxation. Interestingly, the vacancy formation energy for a positive vacancy V_H^+ is substantially lower than that of the negatively charged and neutral vacancies and is most affected by a structural relaxation in which Na atoms neighboring the positively charged vacancy show a distinct outward relaxation. The formation energies of hydrogen vacancies and interstitials in their three charge states are plotted in Fig. 3 as a function of Fermi-level position in the NaH band gap. The zero of the Fermi level is set at the valence-band maximum. Figure 3 shows that the combination of a positively charged vacancy V_H^+ with a negatively charged hydrogen interstitial H_i^-, satisfying the charge neutrality condition, has the lowest formation energy, indicating that this combination is the most probable to occur. However, the formation energy of this vacancy-interstitial pair of 1.53 eV is still too high to explain the high vacancy concentrations and the fast H-D exchange time scales as observed in neutron-diffraction experiments. Further, we calculated the formation energy of an isolated hydrogen vacancy at the NaH(001) surface, since surfaces play an important role in nanoparticles as of their largely increased surface-to-volume ratios. Our calculations show that indeed the energy of creating a neutral vacancy at the NaH surface in its topmost layer is more favorable than in the bulk, with a vacancy formation energy of 0.2 eV below the bulk value. Nevertheless, this effect is too small to account for the observed high hydrogen-vacancy concentrations. Additionally, we also considered vacancy formation at the unrelaxed NaCl//NaH interface at the intermediate Na lattice parameter of 5.10 Å. The formation energy for an isolated neutral vacancy at the interface of 2.53 eV is 5% less than in bulk NaH and still about 2% larger than for a vacancy at the surface.

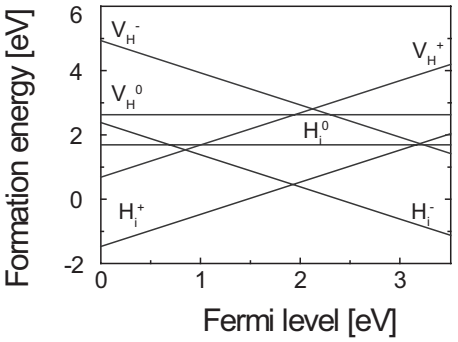

FIG. 3. Calculated formation energies of hydrogen vacancies and interstitials in NaH as a function of Fermi-level position in the band gap. The top of the valence band is taken as the zero of Fermi level.

C. Mechanism for abundant vacancies in nano-NaH

The calculated formation energies described in Sec. III B do not provide a satisfactory explanation for the large vacancy concentrations observed in neutron-diffraction experiments and inferred from the hydrogen-deuterium exchange detected in nano-NaH. We, therefore, evaluated a model which provides a mechanism for the formation of abundant vacancy concentrations in metal hydride nanoparticle (composite) systems.

1. NaCl//Na//NaH growth model

In the $TiCl_3$-doped $NaAlH_4$ system, NaCl is formed simultaneously with NaH in the second desorption step.[6] The small and abundant NaCl crystallites very likely act as nucleation centers for subsequent growth of NaH, since NaH and NaCl share the same rocksalt crystallographic structure and a similar ionic bonding at a fair lattice matching. These factors will promote an easy growth of NaH on NaCl nucleation centers. We examined this by calculating the interface energy for a cube-on-cube growth with NaH(100)//NaCl(100). The lattice mismatches for NaH//NaCl, fcc-Na//NaCl, and fcc-Na//NaH as deduced from our calculations of the respective bulk equilibrium lattice parameters are 13.5%, 6.7%, and 7.3% for the (001)//(001) interfaces. While other orientations, such as NaH(111)//NaCl(200), may provide a better lattice matching, the occurrence of such an interface is not likely, since the atomic bonding is by far less favorable and the resulting interface involves the creation of the energetically unfavorable polar NaH(111) termination. For example, a MgO(100) termination is often observed with the nucleation and growth of embedded nanovoids[29] and nanoparticles[30,31] following ion implantation and thermal annealing, showing its large stability. On the other hand, the unfavorable MgO(111) termination is not detected in the electron microscopy studies.

Still, the relatively largest mismatch (13.5%) for the likely case of cube-on-cube growth of NaH on a NaCl(001) surface indicates that possibly an energetically more favorable growth may occur with the formation of a narrow interlayer of fcc-Na,[32] with a thickness of a few nanometers at most, in between the NaH and NaCl domains, providing a better matching for the subsequent NaCl//Na and Na//NaH interfaces and a lowering of the local strain in the more gradual growth. fcc-Na is expected to stabilize in favor of the bcc structure of bulk Na, because of its good lattice matching, while the difference in cohesive energies is very small. We evaluated whether such a driving force exists to form a narrow interlayer of fcc-Na by calculating the interface energies for the NaCl//NaH, NaCl//Na, and Na//NaH interfaces. The interface energies were calculated in such a way that the induced strain energy due to the lattice mismatch is minimized by a relaxation of the lattice in the direction perpendicular to the interface plane[33] for a set of different fixed lattice parameters in the interface plane. The interface energy is defined as the difference with respect to the energy of the relaxed equilibrium tetragonal bulk systems at a particular fixed lattice parameter in the interface plane.[33]

In this way, we obtained the interface energy for the NaCl(001)//NaH(001) interface of 0.038 J m^{-2}. Similarly, the interface energies for the NaCl//Na and Na//NaH interfaces are 0.24 and 0.28 J m^{-2}, respectively. All these interface energies are quite low, in particular considering the given lattice mismatches, since typical interface energies for cube-on-cube systems with a small lattice mismatch are typically in the range of 1–2 J m^{-2}. For example, the interface energy for a Au(001)//MgO(001) interface, with a small lattice mismatch of approximately 3.2% only, is in the range between 1.5 and 2 J m^{-2}.[34] The interface energies obtained in our calculations give information primarily about the energy needed to form the different chemical bondings of atoms at the interface. Our calculations show that this chemical interface energy is minimum for the NaH//NaCl interface. However, there it is accompanied by a large tetragonal distortion of the NaH lattice to adjust to the NaCl in-plane lattice parameter of 5.47 Å, with a deformation energy of approximately 0.16 eV/NaH pair relative to equilibrium fcc-NaH. On the other hand, while the formation of the NaCl//Na and Na//NaH interfaces requires relatively more energy to create the chemical bonding as compared to the NaH//NaCl interface, here we find that the energy of deformation for Na is very small (roughly 0.008–0.010 eV/Na atom). Na indeed is easily deformable as it has by far the lowest bulk modulus. The value of the bulk modulus is obtained from the equation of state (EOS), which expresses the energy E as a function of the lattice parameter a or volume per Na atom $V=\frac{1}{4}a^3$ for an fcc crystal. The bulk modulus B is defined by Eq. (9) (Ref. 35) evaluated at the calculated fcc equilibrium lattice parameter,

$$B = V\frac{\partial^2 E}{\partial V^2} = \frac{4}{9a}\frac{\partial^2 E}{\partial a^2}. \tag{9}$$

The values for the bulk moduli of NaH, NaCl, and fcc-Na calculated in this way are 26.5, 32.2, and 9.8 GPa, respectively. These values are in close agreement with theoretical and experimental bulk moduli for NaH,[36] NaCl,[37] and Na (Ref. 38) reported in the literature. The large difference in the bulk modulus of Na relative to NaH and NaCl confirms that the formation of an intermediate Na layer will aid significantly to minimize the elastic part of the interface energy as Na is easily deformable. Our calculations indicate therefore that fcc-Na is likely to form in between NaCl and NaH upon growth of Na(H) on top of the NaCl small crystallites as this will lower the overall interface energy needed. Moreover, this also allows for the growth of a more gradual interface region reducing the local strain arising from the larger lattice mismatch between NaCl and NaH.

This leads us to propose that, initially during the second desorption step, fcc Na indeed grows on the NaCl crystallites while maintaining the fcc (rocksalt) crystal structure[32] and subsequently NaH is formed on top. The thin fcc-Na interlayer effectively contains abundant hydrogen vacancies, and because of the high mobility of hydrogen in the fcc-Na lattice, it will provide a pathway for fast hydrogen or deuterium transport toward or from the NaH_{1-x} nanoparticles during H-D exchange or hydrogen sorption processes. The NaCl//Na//NaH growth model, therefore, provides a plausible mechanism explaining the high concentration of hydrogen vacancies[39] and H-D exchange in NaH observed experimentally. A direct consequence is that this will only occur effectively for submicrometer-sized NaH grains and in the presence of NaCl, consistent with currently available experimental data.

IV. CONCLUSIONS

Our calculations clearly show that the presence of hydrogen vacancies significantly affects the hydrogen migration

energy in NaH, resulting in faster diffusion, and enabling H-D exchange in nano-NaH as observed upon decomposition of ball-milled $TiCl_3$-doped $NaAlH_4$. The estimated rate of the vacancy-mediated hydrogen transport based on diffusion theory is consistent with observed H-D exchange reaction rates. The formation energies for intrinsic hydrogen-vacancy-interstitial pairs are too high to explain the observed high hydrogen-vacancy concentrations. We evaluated a model to provide an insight into the mechanisms leading to the presence of abundant hydrogen vacancies. The calculated low fcc-Na//NaCl and NaH//fcc-Na (001) interface energies show that the proposed mechanism to induce abundant hydrogen vacancies by promoting the growth of an fcc-Na interlayer between NaH crystallites and the NaCl nucleation centers is rational. The calculated low interface energies support the view that NaH grows easily on NaCl nucleation centers and assist the idea of the role of NaCl as a grain refiner for NaH.

ACKNOWLEDGMENTS

We acknowledge C. G. van de Walle and M. Wagemaker for providing stimulating discussions. This work was financed within the Sustainable Hydrogen Programme of the Delft Institute for Sustainable Energy (DISE), Delft University of Technology, and benefited from allocation of supercomputer time at SARA (Amsterdam), with financial support from Stichting Nationale Computerfaciliteiten NCF/NWO.

*s.singh@tudelft.nl

[1] L. Schlapbach and A. Zuettel, Nature (London) **414**, 353 (2001).
[2] B. Bogdanović and M. Schwickardi, J. Alloys Compd. **253-254**, 1 (1997).
[3] B. Bogdanović, M. Felderhoff, S. Kaskel, A. Pommerin, K. Schlichte, and F. Schueth, Adv. Mater. (Weinheim, Ger.) **15**, 1012 (2003).
[4] O. Palumbo, A. Paolone, R. Cantelli, C. M. Jensen, and M. Sulic, J. Phys. Chem. B **110**, 9105 (2006).
[5] A. Peles and C. G. Van de Walle, Phys. Rev. B **76**, 214101 (2007).
[6] S. Singh, S. W. H. Eijt, J. Huot, W. A. Kockelmann, M. Wagemaker, and F. M. Mulder, Acta Mater. **55**, 5549 (2007).
[7] S. Singh, S. W. H. Eijt, M. W. Zandbergen, W. J. Legerstee, and V. L. Svetchnikov, J. Alloys Compd. **441**, 344 (2007).
[8] H. G. Schimmel, J. Huot, L. C. Chapon, F. D. Tichelaar, and F. M. Mulder, J. Am. Chem. Soc. **127**, 14348 (2005).
[9] A. Borgschulte, U. Boesenberg, G. Barkhordarian, M. Dornheim, and R. Bormann, Catal. Today **120**, 262 (2007).
[10] M. Wagemaker, W. J. H. Borghols, and F. M. Mulder, J. Am. Chem. Soc. **129**, 4323 (2007).
[11] A. Borgschulte, A. Zuettel, P. Hug, G. Barkhordarian, N. Eigen, M. Dornheim, R. Bormann, and A. J. Ramirez-Cuesta, Phys. Chem. Chem. Phys. **10**, 4045 (2008).
[12] M. Felderhoff *et al.*, Phys. Chem. Chem. Phys. **6**, 4369 (2004).
[13] Q. Shi, J. Voss, H. S. Jacobson, K. Lefmann, M. Zamponi, and T. Vegge, J. Alloys Compd. **446-447**, 469 (2007).
[14] R. J. Borg and G. J. Dienes, *An Introduction to Solid State Diffusion* (Academic, Boston, 1988).
[15] F. A. Kroger, *The Chemistry of Imperfect Crystals* (North-Holland, Amsterdam, 1964).
[16] A. Peles and C. G. van de Walle, J. Alloys Compd. **446-447**, 459 (2007).
[17] P. Hohenberg and W. Kohn, Phys. Rev. **136**, B864 (1964).
[18] W. Kohn and L. J. Sham, Phys. Rev. **140**, A1133 (1965).
[19] D. Vanderbilt, Phys. Rev. B **41**, 7892 (1990).
[20] J. P. Perdew and Y. Wang, Phys. Rev. B **45**, 13244 (1992).
[21] J. P. Perdew, K. Burke, and M. Ernzerhof, Phys. Rev. Lett. **77**, 3865 (1996).
[22] G. Kresse and J. Furthmuller, Phys. Rev. B **54**, 11169 (1996).
[23] H. J. Monkhorst and J. D. Pack, Phys. Rev. B **13**, 5188 (1976).
[24] C. G. Shull, E. O. Wollan, G. A. Morton, and W. L. Davidson, Phys. Rev. **73**, 842 (1948).
[25] W. H. Bragg and W. L. Bragg, *Proceedings of the Royal Society of London: Series A, Containing Papers of a Mathematical and Physical Character* (Royal Society, London, 1913), Vol. 88, No. 605, p. 428.
[26] X. Ke and I. Tanaka, Phys. Rev. B **71**, 024117 (2005).
[27] C. G. van de Walle and J. Neugebauer, J. Appl. Phys. **95**, 3851 (2004).
[28] S. B. Zhang and J. E. Northrup, Phys. Rev. Lett. **67**, 2339 (1991).
[29] B. J. Kooi, A. van Veen, J. Th. M. de Hosson, H. Schut, A. V. Fedorov, and F. Labohm, Appl. Phys. Lett. **76**, 1110 (2000).
[30] C. V. Falub, P. E. Mijnarends, S. W. H. Eijt, M. A. van Huis, A. van Veen, and H. Schut, Phys. Rev. B **66**, 075426 (2002).
[31] S. W. H. Eijt, J. de Roode, H. Schut, B. J. Kooi, and J. Th. M. de Hosson, Appl. Phys. Lett. **91**, 201906 (2007).
[32] A. V. Sugonyako, D. I. Vainshtein, A. A. Turkin, H. W. den Hartog, and A. A. Bukharaev, J. Phys.: Condens. Matter **16**, 785 (2004).
[33] M. Wagemaker, F. M. Mulder, and A. van der Ven (unpublished).
[34] D. Chen, X. L. Ma, and Y. M. Wang, Phys. Rev. B **75**, 125409 (2007).
[35] R. Gaudoin, W. M. C. Foulkes, and G. Rajagopal, J. Phys.: Condens. Matter **14**, 8787 (2002).
[36] S. J. Duclos, Y. K. Vohra, A. L. Ruoff, S. Filipek, and B. Baranowski, Phys. Rev. B **36**, 7664 (1987).
[37] S. R. Elliott, *The Physics and Chemistry of Solids* (Wiley, New York, 1998), p. 193.
[38] Y. Xie, J. S. Tse, T. Cui, A. R. Oganov, Z. He, Y. Ma, and G. Zou, Phys. Rev. B **75**, 064102 (2007).
[39] Assuming a thickness of ~ 1 nm for the fcc-Na interlayer and a contact area of $\sim 10\%$ of the surface of a NaH crystallite ($R \approx 60$ nm) with the neighboring NaCl ($R \sim 20$ nm) nucleation centers leads to an estimated hydrogen-vacancy fraction of $c \approx 0.5\%$.